Temporal and constriction behavior of low-pressure, cathode-dominated argon discharges

Z. Lj. Petrović* and A. V. Phelps
JILA, University of Colorado and National Institute of Standards and Technology, Boulder, Colorado 80309-0440
(Received 19 February 1997)

Measurements of quasi-steady-state voltage-current characteristics, low-current voltage and current oscillations, and constriction formation are reported for cathode-dominated discharges in low-pressure Ar. Pulsed discharges ($\sim$5 ms long at 1–3 Hz) reduce heating and improve the accuracy of differential voltage measurements. Values of pressure p times the separation d of the parallel-plane electrodes are 0.12 to 2 Torr cm corresponding to discharge breakdown voltages of 2 kV to 230 V. Discharge currents range from 2 μA to 40 mA. The quasi-steady-state discharge voltages decrease from their breakdown values in direct proportion to the current, i.e., the negative-differential-voltage-to-current ratio is constant. At currents below the onset of self-sustained oscillations and at the higher pressures, the frequency and damping of transient oscillations are in agreement with a perturbation model based on changes in ion-induced electron emission at the cathode caused by space-charge electric fields. At the higher currents and low pressures transient voltage and current waveforms show the growth of low-frequency oscillations accompanying the onset of constrictions. Rotation of the constricted discharge is observed at these pressures. At the higher pressures the constrictions are stable during the pulse and emission scans parallel to the electrodes provide quantitative data on constricted discharge areas and emissivity per unit current as the discharge increases in size with increasing current. Comparisons are made of these experiments with recent models where possible. [S1063-651X(97)05111-8]

PACS number(s): 52.80.Dy, 52.80.Hc, 52.40.Hf

I. INTRODUCTION

We present measurements and comparisons with existing models of the low to moderate current density behavior of cathode-dominated, low-pressure discharges in Ar. The measurements include the quasi-steady-state, voltage-current characteristics and the behavior of damped oscillations. The measurements and analyses of oscillation data and negative-differential-voltage-current ratio (abbreviated as NDVCR) data are an application to Ar of the techniques used in previous measurements and analyses of low-current, low-pressure discharges in H_2 [1–3]. We also present quantitative analyses of our photographs of constricted discharges [4,5] in low-pressure Ar that we published earlier [6]. A pulsed discharge technique allows measurements of both the transient and quasi-steady-state discharge characteristics, while minimizing the effects of electrode heating and sputtering.

In spite of the large amount of research on moderate- and high-current, low-pressure, cathode-dominated, cold-cathode gas discharges in Ar and Ne [4,7,5,8,9], there has been relatively little work on discharges in parallel-plane geometry for which space-charge effects are small, but not negligible, as is the case for the low-current portion of the work reported here. Previous experiments at such low currents include steady-state, voltage-current characteristics at relatively high pressures [10–15], measurements of the dependence of breakdown voltage on initiating current [16], reports of self-sustained oscillations at low currents [12,14,15,17], and very brief reports of measurements of cathode-fall discharge impedance versus frequency [18–20]. Very recently, measurements of ion energy distributions at the cathodes of low-current, low-pressure Ar discharges have been reported [21] for conditions very similar to those reported here.

Early models of these low-current discharges include the recognition of the effects of space charge by Rogowski and co-workers [22] and of possible multistep ionization by Schade [10], analyses of the differential voltage effects in breakdown experiments by Loeb [23] and by Crowe, Bragg, and Thomas [24], and the pioneering numerical calculations of Ward and co-workers [25,26]. Of particular relevance to the present paper are the analytical models of the differential voltage versus current and oscillations for other rare gases [14,15,27]. Most of the recent numerical calculations [27–30] of the temporal development and spatial characteristics of cathode-dominated discharges in Ar have been made for conditions corresponding to our higher currents.

The study of very-low-current discharges makes possible the determination of volume and surface reaction rate coefficients and probabilities under relatively simple conditions. For these discharges, called ''Townsend'' or dark discharges, Townsend's model of ionization growth by an electron avalanche in a uniform electric field is a good first approximation [4,5,9]. At these low current densities space-charge electric fields are small and readily calculated. The resultant perturbations of the discharge are useful in distinguishing and measuring various nonlinear gas-ionization and electrode phenomena [3]. These same nonlinear phenomena are more important at higher current densities, but are closely coupled with the large space-charge-field effects that greatly complicate the models used to interpret experiments [4,5,9]. Evidence for the need to examine simple discharge situations is the considerable confusion regarding the proper application of collision cross-section data in models of ion transport and gas heating caused by ions and by neutral atoms in the cathode region [31].

Much of the recent work on low-pressure Ar discharges has been motivated by plasma processing applications, such

*Also at Institute of Physics, P.O. Box 57, Belgrade, Yugoslavia.

as semiconductor etching and sputtering deposition of materials [32]. In addition, discharges in Ar and other rare gases serve as a convenient testing ground for models of gas discharge switches, lasers, etc. [33]. Optical emission from Ar is often used as a diagnostic for these discharges [34], where models generally assume that the excitation is only produced by electrons. Experiments within this laboratory have shown [35–37] that this assumption is not valid for discharges with significant cathode-fall voltages ($\geqslant$400 V), e.g., sputtering discharges or high-power, capacitively coupled rf discharges with highly asymmetric electrodes. Recent models of sputtering discharges for materials analysis [38,39] make possible more careful comparisons of models with experiments.

An important aspect of cathode fall experiments and models concerns the development and properties of lateral constrictions of the discharge [4,5,7,40]. We will follow quantitatively the transitions in temporal and spatial behavior of constrictions for currents well below their onset to near their disappearance [1]. This includes observations of the delay in the onset of constrictions and of associated growing oscillations. This extends the work of Klyarfel'd [13,41] who reported delays in the onset of constrictions.

In these experiments we have made only moderate efforts to obtain highly reproducible discharge cathode surfaces. Stable cathode surfaces can be obtained by heavy sputtering [42] or by heating to high temperatures in high vacuum [43]. Our point of view is that we need to learn to work with surfaces having arbitrary characteristics, such as might be found in plasma processing. This approach means that we must make enough different observations of breakdown voltage, current-growth rates, oscillation frequencies, or negative-differential-voltage-current relations, over a wide enough range of pd to be able to extract the effective cathode, anode, and gas parameters. Here p and d are the pressure and the electrode spacing. Of course we do require that the cathode be stable enough to allow the necessary series of experiments.

The apparatus and techniques used in these experiments with low-pressure Ar discharges is reviewed in Sec. II. The differential voltage-current data are presented in Sec. III. Section IV summarizes our damped oscillation data and compares it with a model. The radial spatial scans of emission and their analyses are presented in Sec. V. Brief reports of portions of this work have been given previously [6,44].

II. EXPERIMENT

Figure 1 shows a schematic of the apparatus used for these experiments. The drift tube and the associated circuit for applying dc and pulsed voltages to the discharge are identical to those used previously [1,2]. The discharge tube consists of parallel-plane electrodes surrounded by a closely fitting quartz cylinder and mounted in a bakable, stainless-steel chamber. The quartz and suitable feedthrough insulators prevent long path breakdown and allow operation at pd on the left-hand side of the Paschen curve [4]. The cathode is 78 mm in diameter and is made of gold-plated copper. The central 60 mm of the anode is a quartz window mounted in and electrically insulated from the stainless-steel chamber end plate. The usable diameter of the window is 56 mm. The window is covered with evaporated gold to about 60% transmission. Visual observations indicate that the window transmission is spatially uniform, but no quantitative test of window and/or detector uniformity of response is made. Subsequent tests [45] show that nonuniformities of 20% in the optical transmission produced during evaporation of the gold or by sputtering during the experiment are readily detected visually. The stainless-steel end plate is coated with gold sputtered by the discharge. The nominal spacing between electrodes is 1.04 cm. In the present paper the electrode separation is rounded off to 1 cm when citing experimental pd values. The measured capacitance, including cables, of the cathode at point B to ground is 250 pF and that of the anode at point C to ground is 68 pF. The electrodes do not have the shaped electrodes required for operation at high pd and the maximum useful pd is about 10 Torr cm. The gas pressures are measured with a diaphragm-type manometer with a stated accuracy of $\pm$0.01 Torr, where 1 Torr=133 Pa. The gas samples are taken from high-pressure cylinders with a stated purity of 0.9999. The rate of rise of pressure after overnight evacuation and mild baking is $\approx 10^{-4}$ Torr/h.

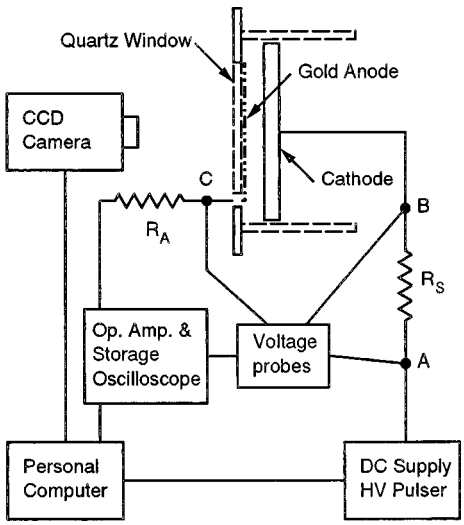

FIG. 1. Schematic of the drift tube, camera, and electrical circuit used for these experiments.

Representative voltage and current wave forms for the pulsed-discharge technique [2,13] used in most of these measurements are shown in Figs. 2 and 3. This pulsed technique has advantages over a continuous or dc discharge because it minimizes gas and electrode heating, reduces sputtering of the cathode, and simplifies the measurement of the differential voltages in the presence of drifting breakdown voltages. Because of the short duration experiments, gas-phase collisions with impurities are not expected to be significant. On the other hand, changes in the cathode surface condition can be large. After aging the cathode with a 10 mA dc discharge in H_2 for 10 min, we are able to run a 2 Torr argon discharge at pulsed currents of up to 50 mA many days with only moderate changes of discharge voltage ($\pm$15 V) and without significant sputtering of cathode material onto the quartz cylinder. On the other hand, ruinous sputtering was encountered during measurements at 0.12 Torr and pulsed voltages and currents $\approx$2000 V and $\sim$10 mA, respectively.

The dc power supply and high-voltage pulser of Fig. 1 supplies a voltage pulse ($\leqslant$1.2 kV) superimposed on a dc voltage ($\leqslant$1 kV), so as to cause a transition from a low-

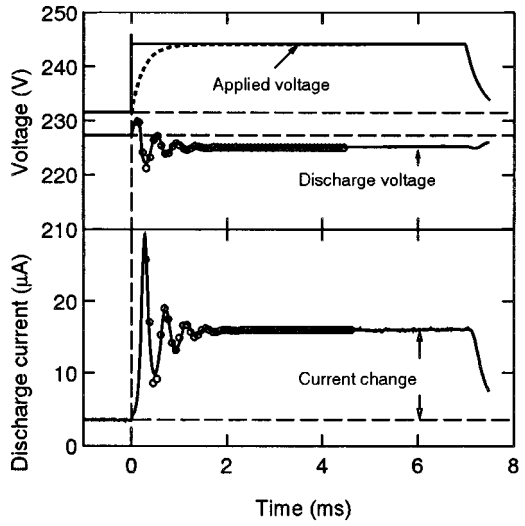

FIG. 2. Representative voltage and current transients resulting from the application of the voltage shown in the upper solid curve to point A in the circuit of Fig. 1 for an Ar pressure of 2 Torr, $R_S=1\ \mathrm{M}\Omega$, $R_A=200\ \mathrm{k}\Omega$, and a breakdown voltage of 228 V. The dotted curve is the voltage at point B when no gas is present. The middle trace shows the voltage across the discharge, while the lowest trace shows the current I through the discharge tube. The solid curves are experimental data and the points show fits of damped sinusoids to the experimental data.

current (2–100 μA) ''keep alive'' discharge to the desired current (0.02–100 mA). The details of the circuit are given in Fig. 1 of Ref. [2]. The dc discharge present between pulses operates at voltages slightly below the breakdown voltage V_b

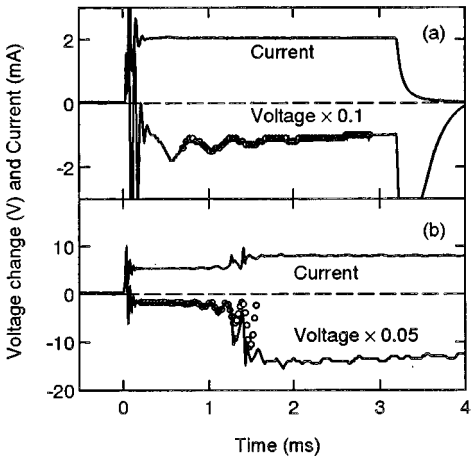

FIG. 3. Representative voltage and current transients resulting from the application of a pulse voltage to point A in the circuit of Fig. 1 for an Ar pressure of 0.12 Torr. In the upper set of wave forms the applied voltage pulse is $\approx$400 V for 3.3 ms, while in the lower case it is $\approx$1000 V for 6.3 ms. The upper trace in each pair shows the current I through the discharge tube, while the lower trace shows the voltage change between the electrodes of the discharge tube. In this case $R_A=0$. These traces show both the high- and low-frequency oscillations. The lower pair of wave forms show that low-frequency oscillations grow until the discharges switch into a constricted mode. The solid curves are experimental data. The points show a fit of damped or growing sinusoid to the data in the vicinity of the transition.

TABLE I. Discharge parameters.

p (Torr)	V_B (V)	E/n (kTd)	γ_i	NDVCR (V/A)	k_I (V/A)
0.12	2050±50	50	0.5	5500	1.502
0.2	1050±10	15.3	0.18	27 000	3.89
0.3	550±35	0.53	0.05	90 000	7.8
2	230±3	0.34	0.01	150 000	42.8

because of the interaction of the series resistor R_A and the negative-differential-voltage versus current characteristic of the discharge [4]. The breakdown voltages vary from 2 kV for a pd of 0.12 Torr cm to 230 V for a pd of 2 Torr cm. See Table I for details. Except as noted, $R_S=200\ \mathrm{k}\Omega$ and $R_A=0$ for pressures of 0.13–0.3 Torr. For some of the 2 Torr data $R_S=1\ \mathrm{M}\Omega$ and $R_A=200\ \mathrm{k}\Omega$, while for other runs these resistors are interchanged. Voltage pulses with measured rise times of about 100 ns followed by an overshoot of $\approx$15% lasting about 50 ns are obtained at point A in Fig. 1. The voltage generated at this point is applied to the discharge tube and its cable and electrode capacitance C (not shown) through the series resistor R_S. The upper solid curve in Fig. 2 shows a calculated voltage wave form at point A [46], while the associated dotted wave form shows the voltage appearing at the discharge tube electrodes in the absence of gas.

The duration of the voltage pulses is roughly 5 ms at a repetition rate of 1–3 Hz. At the highest currents the pulse length is reduced to $\sim$200 μs to reduce the loss of charge from the storage capacitor and the resultant voltage drop. Many of the data sets are obtained with a resistor R_A, used as a current monitor in previous experiments [1,2], inserted between the discharge tube and the operational amplifier, i.e., between the discharge tube and the effective ground. Because of the close proximity of this resistor to the discharge, R_A tends to raise the current threshold for self-sustained oscillations [1]. See Ref. [3] for a model including the effects of R_A. At 2 Torr even with R_A equal to five times the value theoretically required [3] to damp the self-sustained oscillations, there remains a range of currents for which these oscillations are observed. When R_A was significant, as for the 2 Torr data, measurements of difference in voltage at points B and C are used to obtain the discharge voltage.

Fast voltage probes rated at 80 MHz bandwidth are used for measuring the discharge voltage transients. The current and voltage transients are recorded using a 100 MHz storage scope and then are transferred to a personal computer. The voltage scale of the oscilloscope-computer combination is calibrated against a precision voltage supply. Resistors rated at ±2% are used to determine the current.

The charge-coupled semiconductor device (CCD) camera used (black and white Sanyo Model VDC 2624) is mounted as shown in Fig. 1 to record the spatial distribution of emission across the cathode. The spatial resolution estimated from the photographs is better than 0.5 mm. A ''frame grabber'' is used to capture the video signal for processing by the computer. The sensitivity of the camera presumably peaks in the red, but no specifics are available. The camera is operated with its automatic gain control disabled. The data were ana-

lyzed by background subtraction and correction for nonlinearities introduced by the camera electronics. The nonlinearity of the camera is determined by observing the diffused image of a light-emitting diode (LED) driven by a constant-current pulse at a 1 Hz rate as the pulse length is varied from 10 μs to 10 ms. We assume that the CCD elements integrate the photon signal over the LED pulse length. Because the camera exposure time is fixed at 16 ms, the temporal variation of the spatial dependence of emission can be sampled only by turning off the discharge at various times.

The uppermost curve of Fig. 2 shows the applied voltage at point *A* as calculated [46] from the measured currents, voltages, and circuit parameters. The middle solid curve of Fig. 2 is obtained from the voltage difference between points *B* and *C* and the measured dc voltage-current characteristics, while the lower solid curve is the current measured by the operational amplifier. In Sec. III we will summarize the discharge voltage-change observations and then in Sec. IV we summarize the oscillation aspects of the wave forms. Because we do not use the balanced amplifier of Ref. [2] in the present set of experiments, the initial rise in the current wave form is caused by the capacitative coupling of the cathode voltage change and we cannot analyze the initial discharge current growth.

In addition to quasi-steady-state voltage and current changes, the two sets of data of Fig. 3 show the presence of two modes of oscillations. This figure also illustrates the change from a decay of lower-frequency oscillations in Fig. 3(a) to a growth of these oscillations in Fig. 3(b). The latter figure also shows a transition from a low-current and small voltage-change mode to a higher-current and larger voltage-change mode. The frequencies and their damping are discussed in Sec. IV. When a discharge such as that shown in Fig. 3(b) is terminated before the transition in current and voltage, e.g., prior to 1.2 ms, the spatial distribution is visually observed to be diffuse. When the discharge pulse length is extended for all of the wave forms shown, the spatial distribution of emission integrated over all of the pulse is concentrated near the discharge tube wall. We will show in Sec. V B that after the transition to the higher-current mode the constricted discharge rotates.

III. DIFFERENTIAL VOLTAGE VERSUS CURRENT RESULTS

Measurements of the voltage decrease during the quasi-steady-state portion of the pulsed discharges, such as shown in Figs. 2 and 3, are plotted versus the quasi-steady-state current in Fig. 4. In cases where there is a slow change in voltage during the later portions of the pulse, e.g., Fig. 3(a), the wave form is extrapolated back to the beginning of the pulse to obtain the numbers shown. For each pressure these data show a linear portion at low discharge currents to within the scatter of the data, i.e., a constant NDVCR. The definition of the differential voltage used in this paper is the change in discharge voltage from the breakdown voltage or, its equivalent, the discharge operating voltage extrapolated to zero current, while the voltage differences shown are the change from the discharge voltage between pulses to the quasi-steady-state discharge voltage during the pulse. The resultant errors in the differential voltages are small for our

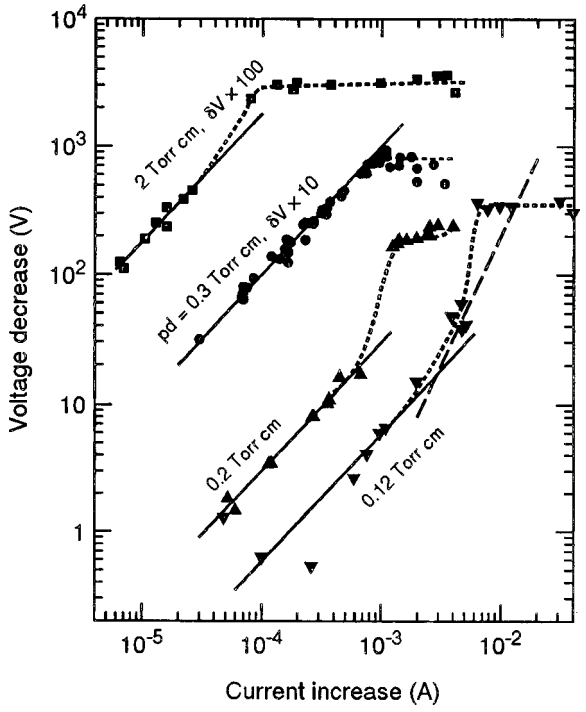

FIG. 4. Voltage decrease vs current increase from measurements such as shown in Figs. 2 and 3. The solid lines assume a constant negative differential voltage to current ratio (NDVCR). The dotted curves connect the regions of constant NDVCR with the constant differential voltage where the discharges are constricted. The dashed line shows the behavior expected for a differential voltage proportional to the square of the current. Note that the voltage decreases for 0.3 and 2 Torr have been multiplied by factors of 10 and 100, respectively. The breakdown voltages corresponding to these data sets are given in Table I.

low discharge maintenance currents. As for low-current discharges in H_2, we have shown [47] that at the higher pressures the constant value for the NDVCR is consistent with space-charge electric-field-induced changes in the net yield of electrons produced by positive ions arriving at the cathode.

As the current during the pulse is increased the voltage decrease begins to rise more rapidly than linearly with current. Eventually the voltage change makes a transition to a region for which the discharge voltage changes very slowly with current. A long history [4,5,8,9] of visual observations of light emission, as well as the quantitative data of Sec. V, show that in the region with a nearly constant voltage the discharge is constricted to a portion of the cathode. Because of the nearly constant voltage and the claim that the current density is constant (see below), the constricted region is often called the *normal glow* region. The gaps in the data of Fig. 4 that occur in the transition region from constant NDVCR to constant voltage correspond to conditions where large amplitude oscillations in the current and voltage prevent us from assigning unique currents and voltages. Although we were often able to suppress these oscillations by increasing R_A [1,3], we could not eliminate them completely.

The upper limit to the current shown for 2 Torr has been extended in other experiments [44] to about 0.1 A. For the purposes of this paper we simply note that the negative differential voltage begins to decrease, i.e., the discharge volt-

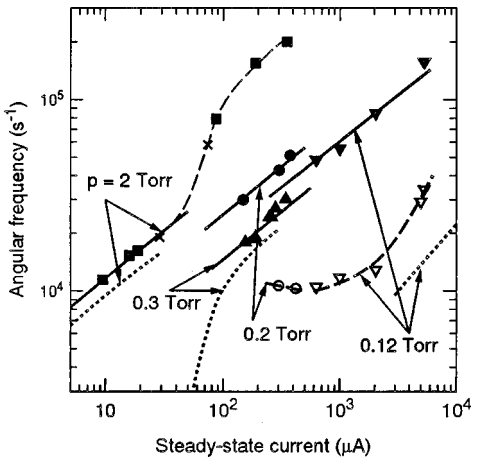

FIG. 5. Angular frequencies obtained from fits to transient voltage and current wave forms vs the quasi-steady-state discharge current. The solid points are from the high-frequency, early-time oscillations, while the open points are from the low-frequency oscillations at later times. The crosses show the frequencies of self-sustained oscillations. The solid lines show the predicted current dependence (not magnitude) of the ion-feedback model of Ref. [3]. The dashed lines simply connect data for 0.12 Torr, for 0.2 Torr, and for 2 Torr. The dotted lines are predictions of the ion-feedback model at 0.12, 0.3, and 2 Torr. Pressures in Torr and associated symbols are 0.12, ▼,∇; 0.2, ●,○; 0.3, ▲; 2, ■.

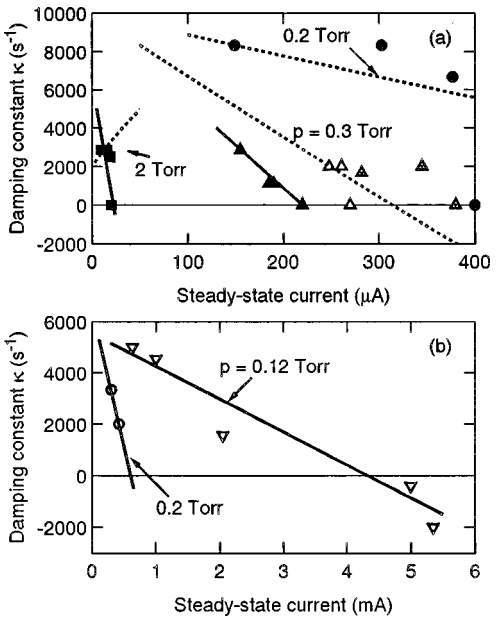

FIG. 6. Damping constants from fits of damped or growing sinusoids to data such as shown in Figs. 2 and 3 vs quasi-steady-state current. The straight lines are drawn through points from a given data set. The dotted lines are damping coefficients predicted with the ion feedback model of Ref. [3]. The solid and open points are from the high-frequency and low-frequency oscillations, respectively. Note the large scatter in the data at the intermediate pressures, especially for 0.2 Torr. The symbols used for the various pressures are the same as in Fig. 5, except that the three different types of upward pointing triangles show results from three different sets of data.

age begins to rise, at currents near 5 mA. This current marks the beginning of the transition to the *above normal* or *abnormal* discharge [4,5]. We will see that this is somewhat below the current at which the cathode would be covered by a uniform glow.

For the case of $p=0.12$ Torr, the dashed line of Fig. 4 shows a quadratic current dependence of the voltage drop, such as that predicted to result from second-order, space-charge electric-field-induced changes in the electron-impact ionization in the discharge gap [3,14,15,27,29]. However, because the value of $\partial^2\alpha/\partial(E/n)^2$ is negative none of these second-order perturbation models is applicable to the lower-pressure, high-E/n data of Fig. 4.

IV. OSCILLATION RESULTS

A. Frequency of oscillations

The experimental voltage and current wave forms of Figs. 2 and 3 show oscillatory behavior representative of low-current, low-pressure pulsed discharges in Ar. The points are fits of damped sinusoids to the data, e.g., Eqs. (1) and (2) of Ref. [2]. The damped oscillations of Figs. 2 and 3 are similar to those obtained previously [1–3] for low-current discharges in H_2. The data of Fig. 3 also show the presence of a low-frequency mode that does not appear to have been reported previously.

The observed angular frequencies ω and damping coefficients κ are summarized in Figs. 5 and 6. Here the solid points are values from data such as shown in Fig. 2 and in the high-frequency, early-time portion of Figs. 3(a) and 3(b). The crosses for 2 Torr show the frequencies of the self-sustained oscillations plotted as a function of the average of the oscillatory current [48]. The three highest-current points for 2 Torr in Fig. 5 are from the low-current portion of the constant voltage region of Fig. 4. The damped oscillations observed at currents above 4×10^{-4} A are too fast to be analyzed with the recording speed used. At currents above 0.1 mA the discharge is constricted and is expected to have a well-developed cathode-fall thickness of roughly one-eighth of the electrode spacing, i.e., a pressure times cathode-fall thickness of about 0.25 Torr cm [4,5]. The resultant shorter ion transit times are expected to result in higher oscillation frequencies at a given current [27,49,50] as observed in Fig. 5.

Because of the low pd values of the present experiments we expect an important feedback mechanism to be ion-induced electron emission from the cathode [4,5,3,9,51]. We therefore compare our results with the predictions of Eq. (20) of Ref. [3] using discharge parameters obtained by fitting the model to our measured breakdown voltages and NDVCR values. See the Appendix for the discharge parameters used in the model. The solid straight lines of Fig. 5 show that the measured angular frequencies ω vary as the square root of the current as predicted by Eq. (20) of Ref. [3] for small currents, $\omega^2 \gg \kappa$, and large R_S. The numerical predictions of the detailed model are shown by the dotted lines for 2, 0.3, and 0.12 Torr. The predictions for 0.2 Torr essentially coincide with the higher current portion of the predictions for 0.3 Torr. The decrease in the dotted curve below the square root behavior at low currents for 0.3 is caused by the approach of ω^2 to κ, i.e., the approach to overdamping [3].

The model predictions are about 20% smaller than experiment at 2 Torr [52] and 0.3 Torr, but are almost an order of

magnitude too small at 0.12 Torr. Note that at 2 Torr a significant contribution from photon feedback would raise the calculated frequencies above the experimental values. Processes of potential importance at very low pressures that have been omitted from the simple ion feedback model are (a) the significant backscattered-electron contribution to ionization [35], (b) the fast-atom induced ionization in the gap [35], (c) fast atom (or ion) excitation of Doppler shifted far-uv resonance photons that are not absorbed by the Ar atoms, (d) fast-atom induced electron emission from the cathode, and (e) the distance required for electrons leaving the cathode to begin to produce ionization [4]. The first four processes cause higher-current growth rates and higher oscillation frequencies and produce ions closer to the cathode with resultant shorter effective ion transit times. The fifth process causes ionization to occur closer to the anode and tends to lower the frequencies. The magnitude of the net contribution is currently unknown. Because of the small number of collisions involved, Monte Carlo calculations including these processes would seem to be the easiest way to evaluate their effects.

The open points for pressures of 0.12 and 0.2 Torr in Fig. 5 are from fits of exponentially damped or growing oscillations to the low-frequency oscillatory portions of wave forms, such as shown in Fig. 3. In some cases the oscillations that grow before the transition are also observed after the transition where they decay to a low amplitude. We know of no valid model applicable at the very high electric field to gas density ratios E/n of the low-frequency oscillations shown in Fig. 3 and summarized in Figs. 5 and 6. The fact that they are associated with the onset of constrictions suggests that they are lateral oscillations, similar to those of the low-E/n model of Kolobov and Fiala [27]. The role of rotation of these constrictions, discussed in Sec. V B, is unknown.

B. Damping of oscillations

Measured damping coefficients κ are shown in Fig. 6 as a function of the quasi-steady-state current. Part (a) of this figure shows κ values from fits of damped sinusoids to the high-frequency oscillations in the current and/or voltage such as shown in Fig. 2 and the very early portions of the wave forms of Fig. 3. The points plotted at zero damping are the currents at which self-sustained oscillations begin. The damping at high frequencies for a pressure of 0.12 Torr is not shown because plotting the very large currents used would compress the low-current data too much. The large scatter in the damping data at 0.3 Torr is probably caused by changes in the cathode electron yield. While scatter in κ values is expected because of drift in the oscillation frequency during the measurement and the resultant erratic cancellation of the later portions of the oscillating wave form [1], there is little scatter in the frequency data at this pressure.

The solid curves in Fig. 6 are chosen to connect data points for a given data set, while the dotted curves are calculated from Eq. (21) of Ref. [3] using discharge parameters presented in the Appendix. As predicted by Eq. (28) of Ref. [3] for high frequencies and small enough currents, the damping data for 0.12 Torr (not shown) scatter about the value $1/(2R_SC)$. The solid line for 0.3 Torr shows how the damping results for one day's data extrapolate to zero near the current threshold for self-sustained oscillations. While the discrepancy between the rising theory curve for 2 Torr and experiment appears serious, it should be noted that a factor of two reduction in the value of R_A used in the model results in reasonable agreement. This suggests that a more accurate model taking into account the capacitance from the anode to ground is required. The calculated damping is not very sensitive to other parameters, i.e., the electron yield γ_i in the ion-feedback model.

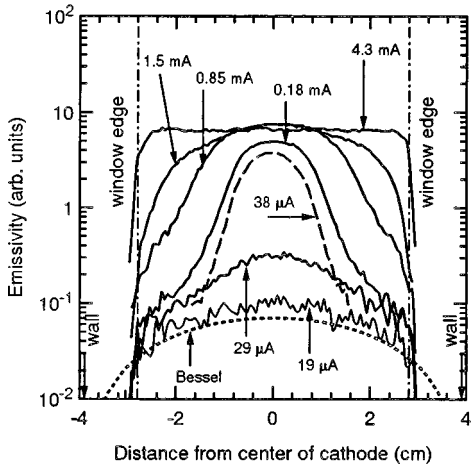

FIG. 7. Emission profiles from near the center of the cathode at a pressure of 2 Torr. The solid curves are averages over several adjacent lines obtained from CCD recordings of emission. The vertical dashed-dotted lines indicate the locations of edges of the semitransparent portion of the anode and the arrows show the position of the quartz wall. The dotted curve is the spatial variation of the emission expected for excited atoms distributed as for the lowest order diffusion mode.

The low-frequency results of Fig. 6(b) show that only for 0.12 Torr are growing oscillations observed with sufficient clarity to obtain quantitative results. Again, we have no model for the damping or growth of the low-frequency oscillations. Unfortunately, the model of Kolobov and Fiala [27] is not applicable at the high E/n for which low-frequency oscillations are observed.

V. CONSTRICTIONS

In this section we present examples of the emission data showing the development of lateral constrictions of low-pressure discharges in Ar. Measurements at 2 Torr provide quantitative emission profiles that are compared with recent models. Measurements at 0.12 and 0.2 Torr show that there is a delay in the onset of a rotating constriction.

A. High pressure

Representative emission profiles for various final pulsed currents at a pressure of 2 Torr are shown in Fig. 7. At this pressure the emission photographs of Ref. [6] show that the discharge constricts to a disk near the center of the electrodes vertically and somewhat to the left horizontally at currents from 85 μA to 4 mA. The relatively small asymmetry of these constrictions shown in the false color pictures of Ref.

[6] may be caused by a tilt of as much as 0.005 rad of the cathode relative to the anode [53]. The positions of the profiles of Fig. 7 are shown by the vertical lines of the photographs of Ref. [6]; i.e., they are along vertical lines passing near the emission maximum. Transient voltage and current wave forms are available for each of these (and other) profiles. Such transient data from other experiments have been reported briefly [54].

At low currents, i.e., for quasi-steady-state values of less than 29 μA, the data of Fig. 7 show that the discharge is diffuse. At 19 μA the discharge emission has roughly a Bessel function spatial distribution as shown by comparison with the dotted calculated curve [55]. For mean currents during the applied voltage pulse from 30 μA to 85 μA the current and voltage wave forms show self-sustained oscillations. There is little change in the shape of the spatial profiles for currents from 30 μA to 0.18 mA. For quasi-steady-state currents from 85 μA to at least 4 mA the current and voltage transients show that the quasi-steady-state discharge voltage is nearly independent of current. At the lower currents the time required for damping the oscillations is ~ 500 μs, while at the higher final currents the transient decays monotonically in <200 μs.

The data of Fig. 7 and the pictures of Ref. [6] show that for currents above 850 μA these constricted discharges are relatively uniform. The area of the bright region grows with current and at our highest current of 4.3 mA the discharge has filled a large part of the cathode. It should be kept in mind that the window diameter is only 72% of that of the cathode so that we have to estimate the discharge area in the outer region. The uncertainties in the relative magnitudes of the profiles are estimated from the scatter in the total emission measurements shown in Fig. 8, i.e., $\pm 20\%$ [56]. This scatter appears to result from drift in the discharge current caused by changing cathode conditions. For currents from 2 to 4 mA the spatial distributions of emission are more complex than those shown, i.e., in addition to the slightly off-center core there is a *C* shaped region of emission extending to near the wall that is of comparable but lower intensity. Remnants of this structure are barely noticeable on the right-hand-side of the 4.3 mA picture of Ref. [6].

Figures 8 and 9 show some of the properties of the constricted discharges derived from the digital photographs of Ref. [6]. In particular, the squares and crosses in the upper portion of Fig. 8 show that the ratio of the total emission to the discharge current is independent of the current. The measured relative values of the total emission (squares) have been multiplied by factors of as much as 1.7 (compared to a maximum of 2) to correct for the estimated portion of the discharge hidden from the camera to yield the crosses. By definition, these ratios are also equal to ratios of the mean emissivity to the average current density. The constancy of these ratios is consistent with the assumption that the excitation process for the observed radiation is a linear function of the current density, i.e., that multistep processes are not important for excitation in our discharges [57]. Note that the current density range (see lower set of points) for currents above 0.1 mA is rather limited. Although this conclusion appears contrary to the findings of Lawler *et al.* [58] for He discharges, we note that their experiments with He were conducted at more than an order of magnitude larger current

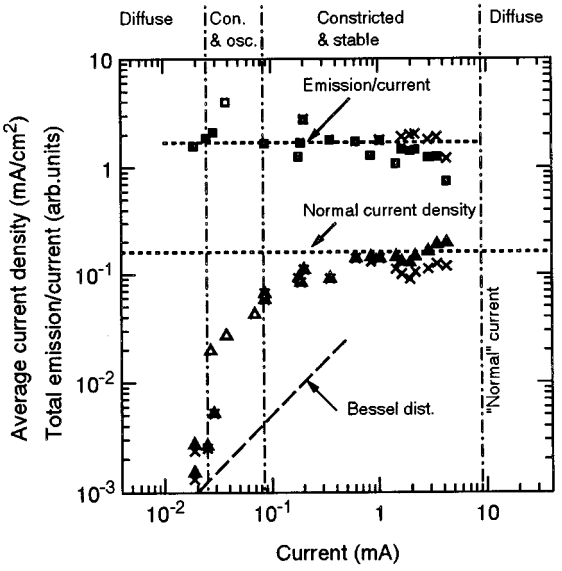

FIG. 8. Measured ratio of the total emission to the current (squares) and of average current density (triangles) for Ar discharges at 2 Torr. The crosses are estimates taking into account emission from the region between the window and the quartz wall. The open points indicate runs where the discharge undergoes self-sustained oscillations during the pulse. The vertical broken lines separate the regions of diffuse, constricted-oscillatory, and constricted-stable discharges. The dotted lines are drawn to indicate trends in the data. The dashed line shows the current density expected for a fundamental diffusion mode (Bessel function) distribution of current.

density than ours. In the remainder of this section we will assume that the emissivity is proportional to the current density and neglect the possibility that the constant ratio of the upper set of data of Fig. 8 is an accident resulting from compensating changes in the efficiency of excitation and in the current density.

The triangles of Fig. 8 show values of the average current density, which is defined as the measured current divided by the area for which the emission exceeds 50% of the peak emission. The crosses show the data after correction for the estimated emission from outside the window opening. This data show that the measured average current density varies by less than 50% as the current is increased through the region of stable constrictions. If the peak value of the current density were constant as the profile changed from roughly that of a Gaussian at ≈ 0.1 mA to a flat-topped profile at ≈ 10 mA we would expect a 30% decrease in the average current density. On the average, the observed $<50\%$ variation the average current density with current is consistent with the claims in the literature [4,5,8,9] that the current density within a constriction is constant as the current increases.

At currents below 0.1 mA, the current density varies rapidly with current. A comparison of the diffuse and oscillatory data for ≈ 28 μA shows that in the oscillatory case the discharge is much more constricted. The values shown for the two lowest currents are subject to considerable uncertainty because of the noisy signals. We have attempeted to reduce the uncertainty by evaluating the peak signal from an aver-

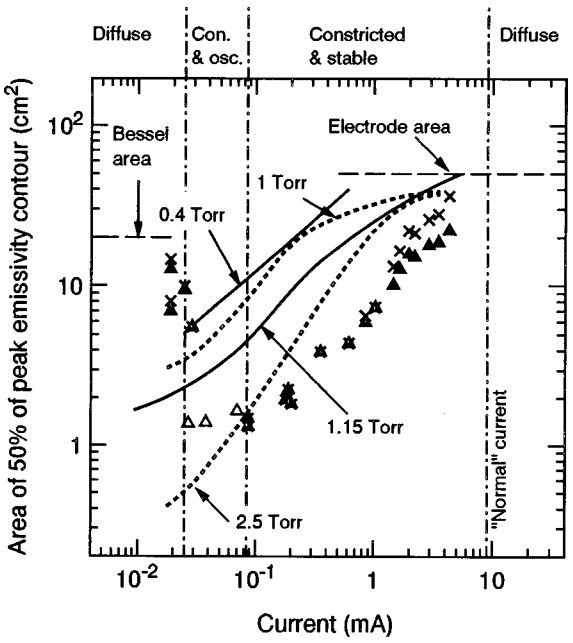

FIG. 9. Area of the 50% intensity contours (triangles and crosses) for Ar discharges at 2 Torr. The crosses, open points, and broken lines are as in Fig. 8. The horizontal dashed lines show the electrode area and the area of the 50% intensity contour expected for a fundamental diffusion mode (Bessel function) distribution of excitation. The dotted curves are scaled from the theory of Holló and Nyirí [29], while the solid curves are scaled from the theory of Fiala, Pitchford, and Boeuf [30].

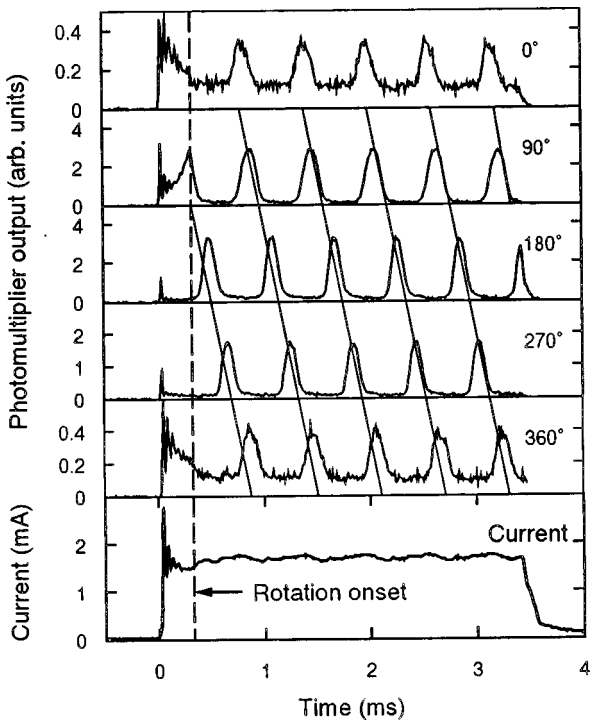

FIG. 10. Emission transients showing rotating constrictions for Ar at 0.2 Torr. The lowest curve shows the corresponding current transient. The emission is observed through apertures located at the angular positions indicated. The vertical dashed line indicates the time of onset of the rotation and the slanted lines allow one to follow the progression of the pattern. Note that the circumferential intensity is highly nonuniform from the beginning of the discharge.

age of the emission data over a small region containing ≈ 50 pixels near the apparent center of the constriction.

The primary purpose of Fig. 9 is to compare our results with recent theoretical predictions [29,30] presented in Sec. V C. The points of Fig. 9 show the current dependence of the areas within which the intensity exceeds 50% of the peak emission. As in Fig. 8, the solid points show data obtained from discharges for which the current and voltage are constant during most of the pulse. The open triangles are averages from runs in which the current and voltage are highly oscillatory. The crosses indicate the areas estimated by extrapolating the observed emission to the quartz wall. Because the emission is not spatially uniform, the correct areas should lie between the triangles and the crosses. Extrapolation of the data of Fig. 9 to the area of the cathode is expected to yield the normal current [4,7,5,8,9] when there are no significant boundary effects near the quartz wall. These data give approximately 9 mA for the normal current and the normal current density of 180 μA/cm^2. Published data [5] give considerably larger values for a typical cathode material, i.e., Fe (Au is not listed). At low currents the area of the 50% emission contour rises toward, but remains below, the value for a Bessel function distribution of exciting electrons.

As was pointed out in connection with Fig. 4 the voltage across the discharge rises significantly at currents between 4 and the 9 mA at the intersection of an extrapolation of the 50% area data and the electrode area in Fig. 9. This effect means that the current at the onset of the abnormal cathode fall depends on the definition of the onset used and so is uncertain by a factor of two.

The labels at the top and the vertical chain lines of Figs. 8 and 9 show the ranges of current for which these discharges in Ar at 2 Torr are in the diffuse, low-space-charge mode; the self-sustained-oscillation mode; the constricted, constant-voltage mode; and in the diffuse, above-normal-current mode. Because of rapid darkening of the window, we did not obtain emission data in the abnormal current region.

Very limited data show spatial distributions similar to those of Fig. 7 for a pressure of 0.3 Torr. As suggested by the roughly flat voltage region in Fig. 4 for 0.3 Torr, constrictions are observed at currents from about 1 mA to at least 3 mA.

B. Low pressure

At 0.12 and 0.2 Torr Ar pressures and at the higher currents the time-integrated CCD camera photographs show the emission to be distributed in a ring near the edge of the window. Ring-shaped emission patterns have been reported for N_2 by Brewer and Miller [59] and by us for H_2 [1]. Figure 10 shows the results of measurements designed to determine whether the observed emission for 0.2 Torr is from a rotating constriction. These experiments use a photomultiplier that detects emission through a 1 in. diameter circular aperture tangent to the edge of the window to observe the emission at four positions 90° apart. The oscilloscope is triggered from the current wave form shown in the bottom trace. Note that the constriction (a) requires about 150 μs to develop, (b) begins at the same circumferential position (90°) over the period of roughly an hour required to obtain the

data, (c) reaches its maximum intensity at $\approx 180°$, i.e., approximately the direction toward which the 2 Torr constrictions are shifted and the suggested location of the distance of closest approach of the electrodes, (d) changes considerably in measured emission signal but not in current (or voltage) as it rotates, and (e) rotates at a frequency about an order of magnitude smaller than that of the low-frequency current and voltage oscillations of Fig. 5. Note that the initial portion of the emission signal varies significantly with circumferential position, and its maximum is near or at the point of initiation of the constriction. Such circumferential nonuniformities of the generally diffuse discharge are shown by pictures (not shown) at 0.2 and 0.12 Torr at currents below those at which constrictions develop. We conclude that the constricted region develops near the wall, i.e., that it essentially touches the quartz wall of the drift tube, and moves along the wall at a roughly constant velocity. It would be useful to examine whether the centering of these low-pressure discharges could be improved by making the electrodes more nearly parallel.

Finally, we present some details regarding the transition to the constricted discharge in the hope that they will aid in the development of a model. For the data set of Fig. 3 at 0.12 Torr the delay of the transition to the constricted form of discharge is observed to decrease from 1.2 to 0.35 ms to 0.2 ms as the current prior to the transition is increased from 5.5 mA to 7.5 mA to 11 mA, respectively. From the measured buildup constant κ and delay time in the data of Fig. 3 the calculated amplitude of the oscillation at the beginning of the pulse is about 1% of the amplitude of the current and voltage change at the transition; i.e., the initial perturbation of the discharge appears small. At 0.2 Torr an initial current of 1.5 mA leads to a delay time of 0.15 ms, as shown in Fig. 10. In several cases at this pressure the initial portions of the current and voltage traces were very noisy. The frequency of the oscillations after the transition, which is more readily determined from the voltage wave form, is initially close to that before the transition. As the pulse continues a stronger component at half this frequency often develops.

C. Comparison with models

Holló and Nyirí [29] have calculated the spatial profiles of the current density of constricted discharges in a dimensionless form that allows scaling to approximately the conditions of our experiments. Their model makes use of simplifications such as the ''local field'' approximation, analytic ionization coefficients, a constant ion mobility, a linear variation of the electric field with distance, and neglect of the higher radial derivatives of the position of the ionization front. The calculated profiles are qualitatively similar to these of Fig. 7, but direct comparisons with those of Fig. 7 are not useful because of differences in parameters and the complexity of the resultant figure. The authors show that for an electrode separation that includes all of the cathode fall [4,5] the scaling varies as pR and I [29], where R is the electrode radius and I is the total discharge current. Note that the usual scaling with the pd, where d is the length of the cathode fall or the electrode separation, is absent because of the simplified model.

We show by the dotted curves of Fig. 9 their predictions of the mean area of the constricted region scaled to our discharge radius. Using the gas discharge scaling parameters discussed in the Appendix, their calculations scale to pressures p of 1 and 2.5 Torr. Thus, the result of the application of their model for our p of 2 Torr should lie between the dotted curves shown and would be significantly higher than our data. We note that their choice of electron yield per ion (0.01) is very close to that we derived from breakdown data and present in the Appendix. Whether the use of a better fit of the dependence of ion mobility on E/n (see Appendix) would improve the fit of theory and experiment is not obvious to us.

An aspect of the constrictions evident in the model Holló and Nyirí [29] is that there is a sheath like decrease in the axial current density near the side wall over 10–15% of the radius. This behavior causes the saturation of the area of the 50% of peak emission contour with increasing current at about 80% of the area of the electrodes. The wall losses causing these sheaths are presumably responsible for the experimentally observed increase in discharge voltage as the discharge area approaches the electrode area as discussed in Sec. V A. Another feature of the model is that at low currents their published spatial solutions apparently do not approach the Bessel function behavior characteristic of the fundamental mode diffusion solution discussed above. This difference is responsible for the failure of the dotted curves of Fig. 9 to rise at low currents, as observed experimentally. The model of Ref. [29] predicts that for the higher pR the mean current density is nearly constant for a wide range of currents as in Fig. 8.

Very detailed models of low-pressure discharges in Ar has been developed by Fiala, Pitchford, and Boeuf [30]. In comparing their predictions with our experiment one must keep in mind that they use the high and constant electron yield per ion expected for a very clean cathode [60]. We assume from Ref. [29] that for an electrode separation that includes all of the cathode fall [4,5] the spatial and current scaling varies as pR and I. Then the areas of the 50% contours estimated from the ionization contours of Figs. 4 and 7 of Ref. [30] scale to the solid curves of Fig. 9 at scaled pressures of 0.4 and 1.15 Torr. Assuming that the predicted areas continue to decrease with increasing pressure p we expect our data for $p=2$ Torr to lie below their predictions, as observed. Although an extension of this model [27] gives the observed approach to the Bessel function spatial distribution behavior at low currents, we see no evidence of a minimum area in the limited number of cases solved. Because many of the recent and detailed models [30,33] of the cathode fall are for much more complicated electrode geometries than ours, comparisons with our experiments are not possible.

VI. DISCUSSION

The experimental results presented in this paper provide some of the quantitative data needed to test the large number of computer codes being developed to describe low-pressure electrical discharges [30,33,38,39]. Verification of these codes in the relatively ideal geometry and wide range of experimental parameters of our experiments offers the possibility of separating out the various contributions to gas ionization, electron emission from the cathode, electron back-

scattering from the anode, and heavy particle collisions. The simple geometry also makes it easier to test for the effects of space-charge electric fields at low currents and to test scaling laws at all currents.

The measurements at low currents of the negative-differential-voltage-current ratio and of the frequency and damping of transient oscillations in the voltage and current wave forms presented in Secs. III and IV provide a test of the applicability of models of the nonlinear ionization and feedback processes in an Ar discharge. In particular, we find that a model assuming the dominant nonlinear effect is the change in ion-induced electron emission at the cathode caused by space-charge enhancement of the electron yield explains the experimental oscillation results at 2 and 0.3 Torr cm rather well. This model is the same as that used successfully to explain the oscillations in current and voltage for low-current, low-pressure discharges in H_2 [3]. At 0.12 and 0.2 Torr cm this model fails to explain the observed oscillation frequencies by a large factor and we do not yet have a convincing explanation.

At discharge currents below the normal current we used spatially dependent emission measurements as well as current and voltage wave forms to follow quantitatively the transition from diffuse discharges to constricted discharges. We find that the average current density within a constriction is approximately constant as claimed in the literature on the basis of very limited data. Our data for Ar show that the mean emissivity is a linear function of the average current density, as expected for single-step excitation of the emission. This observation is in contrast to, but consistent with, the two-step excitation reported for the cathode region of He discharges at current densities an order of magnitude higher.

The comparison of experiments with recent models of constrictions is limited by the problems of scaling the models to the experiment. The model of Holló and Nyirí [29] is in semiquantitative agreement with our experiments except at low currents where space-charge effects are small and the model apparently does not approach the fundamental diffusion mode solution. In view of the simplicity of the model the fit to experiment is surprisingly good. The model of Fiala, Pitchford, and Boeuf [30] predicts the general trend of our data, but needs to be extended to higher pressures and discharge radii and to a lower electron yield per ion at the cathode for a more direct comparison with our experiment.

ACKNOWLEDGMENTS

We would like to acknowledge helpful advice and the loan of equipment by A. Gallagher and R. Hart and helpful discussions with B. M. Jelenković. We thank J. Feeney and R. A. Mitchel for help with the personal computer. The work was supported in part by the Air Force Wright Laboratories, the National Institute of Standards and Technology, and the U.S.-Yugoslavia Joint Board, Project No. 926.

APPENDIX: DISCHARGE CONDITIONS

Here we summarize the discharge parameters required for the model of ion feedback, i.e., by Eqs. (20) and (21) of Ref. [3], when used to calculate the frequencies of Fig. 5 and damping constants of Fig. 6. These parameters are the spatial ionization coefficient, the effective yield of electrons per ion arriving at the cathode, the rate of change of this yield with discharge current, and the ion drift velocity. In this model the escape probability for electrons emitted from the cathode is included in the effective yield expression. We use the circuit resistances and capacitance discussed in Sec. II. We also summarize the parameters used in Sec. V C to scale the models of constrictions to our experiments.

The empirical formula for the spatial (Townsend) ionization coefficient α_i normalized to the gas density n is

$$\begin{aligned}\alpha_i/n = {} & 5\times10^{-21}\exp[-170/(E/n)] \\ & +3\times10^{-20}\exp[-700/(E/n)] \\ & -1.5\times10^{-20}\exp[-10000/(E/n)],\end{aligned} \tag{A1}$$

where E/n is the ratio of the electric field at breakdown to the gas density in Td and $1\ \mathrm{Td}=10^{-21}\ \mathrm{V\,m^2}$.

The ionization coefficients given by Eq. (A1) are used to calculate the effective yield of electrons per ion arriving at the cathode γ_i using the condition that at breakdown the product of the excess electron multiplication and the yield equal unity [4] or that

$$\gamma_i = 1/[\exp(\alpha_i d)-1], \tag{A2}$$

where d is the electrode separation. The results of these calculations are given in Table I. It is convenient to approximate these results by

$$\gamma_i = \{0.01+0.64[(E/n)/30000]^{1.3}/[1+(E/n)/30000]\}. \tag{A3}$$

This approximation is good to $\pm 15\%$. In Eq. (A3) the E/n values are those at the cathode; i.e., we assume that the ion mean-free-path ion is small enough that ion energy is determined by the local electric field at the cathode. It must be kept in mind that the electron yields discussed here are effective values that include contributions from fast Ar atoms produced in charge-transfer collisions of Ar^+ with Ar and reaching the cathode with significant energy [31,38,39,61,36]. This fast atom contribution is expected to be large at the higher E/n of Table I. Equation (A3) is used to calculate the electric field or voltage-dependent portion of Eq. (8) of Ref. [3].

A second parameter in Eq. (8) of Ref. [3] is that of $k_I = \partial\gamma_i/\partial I$. In the present calculations we have obtained k_I from measured values of the NDVCR using Eq. (23) of Ref. [3]. Results are given in Table I. The experimental NDVCR values have previously been compared with predictions of the ion-feedback and other models [47].

The final discharge parameter needed for the ion-feedback model of Ref. [3] is the ion drift velocity W_+. An analytic approximation to the values of Ref. [62] for a wide range of E/n is

$$W_+ = 4(E/n)/[1+0.007(E/n)^{1.5}]^{1/3}. \tag{A4}$$

In order to make comparisons with the model of Holló and Nyirí we need to find approximations to the ionization coefficient and ion drift velocity that follow their adopted

functional form. We have approximated Eq. (A1) in the E/n range of our 2 Torr experiments by

$$\alpha_i/n = 3.1\times 10^{-20}\ \exp[-500/(E/n)] \tag{A5}$$

and have approximated the ion drift velocity by

$$W_+ = 2.5(E/n). \tag{A6}$$

where the units are as given above. Equation (A5) is a reasonably good fit to experiment for the needed range of E/n, but Eq. (A6) has the wrong dependence on E/n and is valid only for a narrow range of E/n.

These parameters are used as follows: the coefficients appearing in Eqs. (A5) and (A6) are used to calculate the values of pR and I from the parameters α and $I\alpha^2$ of the numerical calculations. Then the theoretical values of pR are scaled to our radius of 3.9 cm to obtain the scaled pressures shown in Fig. 9. The discharge areas calculated from the 50% radius of the theoretical current density profiles in Figs. 5 and 6 of Ref. [29] were multiplied by the square of the ratio of our electrode radius to their dimensionless radius of 2 units.

[1] Z. Lj. Petrović and A. V. Phelps, Phys. Rev. E **47**, 2806 (1993).

[2] B. M. Jelenković, K. Rózsa, and A. V. Phelps, Phys. Rev. E **47**, 2816 (1993).

[3] A. V. Phelps, Z. Lj. Petrović, and B. M. Jelenković, Phys. Rev. E **47**, 2825 (1993). Since the publication of this reference, we have realized that the assumption of local-equilibrium made in Sec. IV A is overly restrictive. It should be replaced by assumption (vi) of Sec. III that the spatial distribution of ionization events can be approximated by an exponential growth from the cathode toward the anode. The electron transit time is so short compared to times of interest that we are not concerned with whether the mean velocity and/or energy of the electron is constant. Monte Carlo calculations for N_2 by V. D. Stojanović and Z. Lj. Petrović (unpublished) and for H_2 by Jelenković and Phelps (unpublished) show that the exponential growth approximation is satisfactory for these gases and suggest its use for Ar.

[4] M. J. Druyvesteyn and F. M. Penning, Rev. Mod. Phys. **12**, 87 (1940).

[5] G. Francis, Handb. Phys. **22**, 53 (1956). The very limited current density measurements for constricted discharges are summarized on p. 94. The normal current densities are given on p. 89.

[6] Z. Lj. Petrović and A. V. Phelps, IEEE Trans. Plasma Sci. **24**, 107 (1996).

[7] R. M. Chaudhri and M. A. Baqui, Proc. Phys. Soc. London **65**, 324 (1952). The technique used here is suspect because any nonuniformities of the cathode surface move with the rotating cathode.

[8] G. F. Weston, *Cold Cathode Glow Discharge Tubes* (Iliffe, London, 1968), Chap. 3.

[9] Yu. P. Raizer, *Gas Discharge Physics* (Springer-Verlag, Berlin, 1991), Chap. 8. See also Yu. P. Raizer, Teplofiz. Vys. Temp. **24**, 984 (1987) [High Temp. **24**, 744 (1987)].

[10] R. Schade, Z. Phys. **105**, 595 (1937); **108**, 353 (1938).

[11] H. Büttner, Z. Phys. **111**, 750 (1939).

[12] M. Hayashi, Bull. Nagoya Univ. Dept. of General Education **4**, 131 (1960); M. Hayashi, Bull. Nagoya Inst. Technol. **13**, 334 (1962).

[13] B. N. Klyarfel'd, L. G. Guseva, and A. S. Pokrovskaya-Soboleva, Zh. Tekh. Fiz. **36**, 704 (1966) [Sov. Phys. Tech. Phys. **11**, 520 (1966)].

[14] V. N. Melekhin and N. Yu. Naumov, Zh. Tekh. Fiz. **54**, 1521 (1984) [Sov. Phys. Tech. Phys. **29**, 888 (1984)]; V. N. Melekhin, N. Yu. Naumov, and N. P. Tkachenko, *ibid.* **57**, 454 (1987) [*ibid.* **32**, 274 (1987)].

[15] I. D. Kaganovich, M. A. Fedotov, and L. D. Tsendin, Zh. Tekh. Fiz. **64**, 22 (1994) [Tech. Phys. **39**, 241 (1994)].

[16] R. Schade, Zh. Tekh. Fiz. **18**, 595 (1937).

[17] Dj. A. Bošan, V. Ž. Zlatić, and B. J. Mijović, J. Phys. D **21**, 1462 (1988).

[18] P. Davy, in *Proceedings of the Sixth International Conference on Ionization Phenomena in Gases, Paris, 1963*, edited by P. Hubert and E. Crémieu-Alcan (S.E.R.M.A., Paris, 1963), Vol. 2, p. 99.

[19] C. Yeh, J. Appl. Phys. **27**, 98 (1956).

[20] G. Ashmann and H. J. Oskam, J. Appl. Phys. **29**, 1768 (1958).

[21] M. V. V. S. Rao, R. J. Van Brunt, and J. K. Olthoff, Phys. Rev. E **54**, 5641 (1996).

[22] W. Rogowski and A. Wallraff, Z. Phys. **102**, 183 (1936); W. Rogowski, *ibid.* **114**, 1 (1939).

[23] L. B. Loeb, Rev. Mod. Phys. **8**, 267 (1936); A. von Engle, Handb. Phys. **21**, 504 (1956).

[24] R. W. Crowe, J. K. Bragg, and V. G. Thomas, Phys. Rev. **96**, 10 (1954).

[25] A. L. Ward, Phys. Rev. **112**, 1852 (1958).

[26] A. L. Ward and E. Jones, Phys. Rev. **122**, 376 (1961).

[27] V. I. Kolobov and A. Fiala, Phys. Rev. E **50**, 3018 (1994). We find that at 2 Torr, Eq. (19) of this reference gives a decrease of the differential discharge voltage that is proportional to the square of the current in agreement with the sign of the experimental voltage changes shown in Fig. 4. However, for 0.12 and 0.2 Torr the predicted quadratic voltage change has the wrong sign. One possible reason is that these authors assume that the product of the ionization coefficient and the gap spacing $\alpha_i d \gg 1$, whereas the calculated and measured [54] $\alpha_i d$ value at low pressures is ~ 1.

[28] Yu. P. Raizer and S. T. Surzikov, Pis'ma Zh. Tekh. Fiz. **13**, 452 (1987) [Sov. Tech. Phys. Lett. **13**, 186 (1987)].

[29] S. Holló and B. Nyíri, Acta Phys. Hung. **72**, 71 (1992). The scaling variables we have used, i.e., pR and I, are equivalent to the variables pR and $I/(pR)^2$ used by these authors and to the variables pR and J/p^2, where J is the average current density, often used in discharge models [4,5]. In Fig. 9 we have not shown the area of the contour at the mean current density for the lowest currents in their Figs. 5 and 6 because of the difficulty in reading their graph at low currents. These

authors find damped and growing oscillations at low currents, but do not give sufficient data for us to make comparisons with our experimental oscillations.

[30] A. Fiala, L. C. Pitchford, and J. P. Boeuf, Phys. Rev. E **49**, 5607 (1994). See Figs. 4(b) and 7(b) of this reference. The radii for the area calculations of our Figs. 8 and 9 are at the intersection of the 50% contours and planes through the peak values of the ionization rate and parallel to the electrodes. Possibly integration along the axial direction to simulate experiment more closely would lead to somewhat smaller radii.

[31] A. V. Phelps, J. Appl. Phys. **76**, 747 (1994).

[32] M. A. Lieberman and A. J. Lichtenberg, *Principles of Plasma Discharges and Materials Processing* (Wiley, New York, 1994), Chap. 1.

[33] J.-P. Boeuf and L. C. Pitchford, IEEE Trans. Plasma Sci. **19**, 286 (1991).

[34] S. Djurović, J. R. Roberts, M. A. Sobolweski, and J. K. Olthoff, J. Res. Natl. Inst. Stand. Technol. **98**, 159 (1993).

[35] A. V. Phelps and B. M. Jelenković, Phys. Rev. A **38**, 2975 (1988).

[36] D. A. Scott and A. V. Phelps, Phys. Rev. A **43**, 3043 (1991).

[37] K. Rózsa, A. Gallagher, and Z. Donkó, Phys. Rev. E **52**, 913 (1995).

[38] A. Bogaerts and R. Gijbels, J. Appl. Phys. **78**, 6427 (1995). The large atom-atom cross sections used in this paper have been replaced by lower values. See A. Bogaerts, R. Gijbels, and W. J. Goedheer, Anal. Chem. **68**, 2296 (1996).

[39] A. Fiala, L. C. Pitchford, J. P. Boeuf, and S. Baude, Spectrochim. Acta B **52**, 531 (1997).

[40] K. G. Emeleus, Int. J. Electron. **51**, 269 (1981). This paper contains references to a number of papers on constricted discharges by Emeleus and co-workers.

[41] B. N. Klyarfel'd, Z. Phys. **38**, 289 (1926); **60**, 379 (1930).

[42] F. M. Penning and J. H. A. Moubis, Philips Res. Rep. **1**, 119 (1946); F. M. Penning and J. H. A. Moubis, Physica (Amsterdam) **15**, 721 (1949).

[43] J. P. Molnar, Phys. Rev. **83**, 940 (1951).

[44] Z. Lj. Petrović and A. V. Phelps, Bull. Am. Phys. Soc. **39**, 1490 (1994).

[45] B. M. Jelenković and A. V. Phelps, Bull. Am. Phys. Soc. **39**, 1490 (1994).

[46] Because the voltage at point A was not recorded for this run, the magnitude of the voltage pulse is calculated from $(R_S+R_A)I(t)+$the increase in discharge voltage evaluated near the end of the current pulse. The changes in discharge voltage with current from the assumed breakdown value are taken from the measurements reported in Fig. 4. The time constant used for the calculation of the dotted curve is obtained from separate measurements with no discharge. The whole voltage pattern scales in magnitude as the breakdown voltage changes with cathode conditioning.

[47] A. V. Phelps, in *Proceedings of the XXII International Conference on Phenomena in Ionized Gases*, edited by K. H. Becker, W. E. Carr, and E. E. Kunhard (Stevens Institute of Technology, Hoboken, 1995), p. 107.

[48] All of the measurements reported in this paper are obtained by increasing the current. When the current is decreased through this region there is a hysteresis effect in which the voltage remains constant to lower currents than shown in Fig. 4 and then decreases to the constant NDVCR line shown. We are not concerned with this transition.

[49] G. Ecker and K. G. Müller, Institüte für Theoretisch Physik der Universität Bonn, Technical Report No. FTR 2, 1961 (unpublished). This very useful review was also issued as U.S. Army Report No. DA-91-591-EUC-1254, 1961 (unpublished).

[50] G. Ecker, W. Kröll, and O. Zöller, Ann. Phys. (Leipzig) **15**, 60 (1965).

[51] A. V. Phelps (unpublished).

[52] The data shown in Fig. 5 for 2 Torr are for $R_S=1\ \mathrm{M}\Omega$ and $R_A=200\ \mathrm{k}\Omega$. When these resistors are reversed the measured frequencies at currents below 30 μA increase by about a factor of 2 and the damping coefficients shift to larger currents by about 50%. The change in frequency is in good agreement with the predictions of Eqs. (20) of Ref. [3]. However, the agreement between the predicted and measured damping constant is no better than for the data shown in Fig. 6.

[53] During final disassembly of this apparatus the electrodes were found to be 0.4 mm closer on the left side of the pictures of Ref. [6] than on the right side. This corresponds to an electrode tilt of 0.005 rad. This difference decreases when neoprene gaskets used to protect the quartz are compressed sufficiently to seat the electrode spacers. The effects of the tilted electrodes on emission were investigated in Ref. [45]. The results suggest a comparable deviation from parallelism during the present measurements. The tilt angle cited here is significantly smaller than the upper limit cited in Ref. [15].

[54] B. M. Jelenković and A. V. Phelps, Bull. Am. Phys. Soc. **38**, 2359 (1993).

[55] The Bessel function in Fig. 7 is not fitted to the experimental data so as to make it more easily seen.

[56] An additional uncertainty in the magnitude of the 4.3 mA data of Fig. 7 of $\pm 20\%$ results from an uncalibrated reduction in the camera iris diameter for the higher currents. We have adjusted the relative magnitudes of the camera sensitivity such that averages of the two sets of data for the total emission per unit current of Fig. 8 agree in the region of overlapping currents.

[57] A word of caution is needed here. When we evaluate the ratio of the sum of the squares of the emission signals to the sum of the emission signals the result increases less rapidly than the linear function of the current expected for an excitation process that is linear in current density. This test gives more emphasis to the high-intensity regions of the cathode glow. A possible reason for departures from linearity of the various tests is a change in the cathode-fall thickness with accompanying changes in the electron energy distribution. This test was suggested by A. Gallagher.

[58] J. E. Lawler, E. A. Den Hartog, and W. N. G. Hitchon, Phys. Rev. A **43**, 4427 (1991).

[59] A. K. Brewer and R. R. Miller, Phys. Rev. **42**, 786 (1932). The variation with pressure at fixed current of the spatial distributions of emission found for discharges in nitrogen are qualitatively similar to ours.

[60] H. D. Hagstrum, Phys. Rev. **96**, 325 (1954).

[61] H. Neu, Z. Phys. **154**, 423 (1959); **155**, 77 (1959).

[62] A. V. Phelps, J. Phys. Chem. Ref. Data **20**, 557 (1991). It should be noted that in the absence of more detailed data the total inelastic cross sections in this series of papers should be used with a differential scattering cross section peaked in the forward direction, as is typical of high energy collisions. An isotropic model leads to excessive angular scattering.